AD_____

Award Number: W81XWH-10-1-0112

TITLE: Epithelial and Stromal Spectral Imaging for Rapid Surgical Margin Analysis

PRINCIPAL INVESTIGATOR: Ashley Laughney

CONTRACTING ORGANIZATION: Dartmouth College
Hanover, NH 03755-1404

REPORT DATE: March 2012

TYPE OF REPORT: Annual Summary

PREPARED FOR: U.S. Army Medical Research and Materiel Command
Fort Detrick, Maryland 21702-5012

REPORT DOCUMENTATION PAGE

Form Approved
OMB No. 0704-0188

1. REPORT DATE	2. REPORT TYPE	3. DATES COVERED
March 2012	Annual Summary	1 March 2011 – 28 February 2012

4. TITLE AND SUBTITLE
Epithelial and stromal spectral imaging for rapid surgical margin analysis

5a. CONTRACT NUMBER

5b. GRANT NUMBER
W81XWH-10-1-0112

5c. PROGRAM ELEMENT NUMBER

6. AUTHOR(S)
Ashley Laughney, Venkataramanan Krishnaswamy, Keith Paulsen, Brian Pogue

E-Mail: ashley.laughney@dartmouth.edu

5d. PROJECT NUMBER

5e. TASK NUMBER

5f. WORK UNIT NUMBER

7. PERFORMING ORGANIZATION NAME(S) AND ADDRESS(ES)

Dartmouth College
Hanover, NH 03755-1404

8. PERFORMING ORGANIZATION REPORT NUMBER

9. SPONSORING / MONITORING AGENCY NAME(S) AND ADDRESS(ES)
U.S. Army Medical Research and Materiel Command
Fort Detrick, Maryland 21702-5012

10. SPONSOR/MONITOR'S ACRONYM(S)

11. SPONSOR/MONITOR'S REPORT NUMBER(S)

12. DISTRIBUTION / AVAILABILITY STATEMENT
Approved for Public Release; Distribution Unlimited

13. SUPPLEMENTARY NOTES

14. ABSTRACT
A new, *scanning beam* spectroscopy platform was developed to dramatically improved image acquisition speed of localized light scattering. The new scanning *in situ* spectroscopy platform samples broadband reflectance from a 150μm diameter spot over a 1cm^2 field using a dark field geometry and telecentric lens; the system was designed to balance sensitivity to stromal and epithelial distributions, while sufficiently imaging the inherent diversity within a diagnosis. The diagnostic performance of this new imaging system was tested in 29 tissues procured during breast conservative surgery. Nearly 300,000 broadband spectra were parameterized using light scattering models and spatially dependent spectra signatures were interpreted using co-occurrence matrix representation of image texture. Local scattering changes distinguished benign from malignant pathologies with 94% accuracy, 85% sensitivity, 100% specificity, and 100% positive & 90% negative predictive value, using a threshold-based classifier. Texture and shape features offered unique information about scattering ultra-structures, and suggest a potential contrast mechanism for ductal carcinoma in situ. Images of localized scattering readily identify benign and malignant pathologies in resected specimens and offer new spectral-spatial signatures of clinically relevant breast pathologies.

15. SUBJECT TERMS
None provided.

16. SECURITY CLASSIFICATION OF:			17. LIMITATION OF ABSTRACT	18. NUMBER OF PAGES	19a. NAME OF RESPONSIBLE PERSON
a. REPORT	b. ABSTRACT	c. THIS PAGE			USAMRMC
U	U	U	UU	18	19b. TELEPHONE NUMBER *(include area code)*

Table of Contents

Page

Introduction…….……..….. 1

Body……2-11

Key Research Accomplishments…….……..12

Reportable Outcomes……13

Conclusion……14

References……15

Introduction

Diagnostic sensing of cancer-involved tissues during breast conserving surgery is clinically needed to aid surgeons in achieving complete resection at the time of primary excision. Breast conserving therapy, which includes local tumor excision and radiation therapy, is the standard of care for patients with early invasive breast cancers and for patients with advanced disease whose tumor burden is successfully reduced with neo-adjuvant therapy; it is equally safe and effective as mastectomy when surgical margins are clear of residual disease. Margin assessment is routinely performed post-operatively by histological processing; resulting in a 20-40% re-excision rate and the added risks, cost and psychological effects associated with secondary surgery. The work achieved in year two of this Depart of Defense Pre-doctoral Traineeship Award focused on translation of the prototype system tested in year one of funding to the clinical setting. A new, *scanning beam* spectroscopy platform was developed and tested to dramatically improved image acquisition speed of localized light scattering. The new scanning *in situ* spectroscopy platform samples broadband reflectance from a 150μm diameter spot over a $1cm^2$ field using a dark field geometry and telecentric lens; the system was designed to balance sensitivity to stromal and epithelial distributions, while sufficiently imaging the inherent diversity within a diagnosis. The diagnostic performance of this new imaging system was tested in 29 tissues procured during breast conservative surgery. Nearly 300,000 broadband spectra were parameterized using light scattering models and spatially dependent spectra signatures were interpreted using co-occurrence matrix representation of image texture. Local scattering changes distinguished benign from malignant pathologies with 94% accuracy, 85% sensitivity, 100% specificity, and 100% positive & 90% negative predictive value, using a threshold-based classifier. Texture and shape features were important to optimally discriminate benign from malignant tissues, including pixel-to-pixel correlation, contrast and homogeneity, and the shape features of fractal dimension and Euler number. Analysis of the region-based diagnostic performance revealed that a $1mm^2$ area captured the morphological diversity observed in typical breast pathologies at this sampling resolution, rendering a more robust separation of scattering features. Images of localized scattering readily identify benign and malignant pathologies in resected specimens and offer new spectral-spatial signatures of clinically relevant breast pathologies.

Body

Task 1. Assemble and parameterize an extensive databank of scatter spectra from fresh breast tissue across clinically relevant diagnostic categories.

Surgical breast tissues, both lumpectomy and biopsy specimens, were imaged with a custom-built, scanning-beam spectroscopy platform. A schematic of the system is presented in Figure 1 and is described elsewhere in the literature [1].

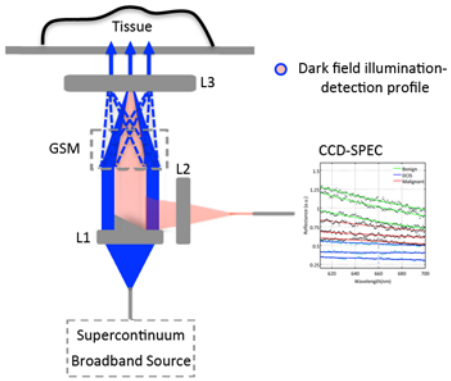

Figure 1 Schematic of the scanning in situ spectroscopy platform

In brief, the imaging system employs dark-field illumination and locally detects broadband spectra (450:700nm) at 150μm lateral resolution over a 1cm2 field-of-view (FOV). A broadband, telecentric, f-theta lens with a scanning mirror is used to rapidly pass the illumination beam across the tissue surface without mechanically translating the specimen or imaging system. Each tissue sample is mounted on a glass plate above the optical assembly and dense spectral imaging is performed in a non-contact and inverted geometry. Non-contact sampling avoids reflectance profile changes induced by probe contact pressure, a significant artifact quantified by Ti[2]. Measurement time per sample is substantially improved, as compared to DAQ with our static-beam prototype (12 minutes as compared to 1hr). Trace background reflection from the optical system, $R_{BG,meas}(x,y,\lambda)$, were acquired and subtracted from the measured spectra, $R_{TISSUE,meas}(x,y,\lambda)$, and data were normalized to the spectral response of the system, $R_{SPEC,meas}(x,y,\lambda)$, on a pixel-by-pixel basis using a 5% diffuse reflectance Spectralon standard (SRS-05-010 Labsphere, Inc., Northern Sutton, New Hampshire). Spectralon standards are highly stable, providing a daily calibration for direct comparison between tissue samples; this model number was chosen because it presented a similar reflectance level to the tissues imaged. While the standard can be calibrated to absolute coefficients of absorption and reduced scattering, a light transport model is required for our complex sampling geometry. Hence, calibration was not performed because it only results in a linear scaling of the recovered scattering parameters. Background, reference and sample measurements were acquired without

removing the glass sample holder from the optical assembly, and produced a reflectance measure relative to the Spectralon standard according to

$$R_{TISSUE,ref}(x,y,\lambda) = \frac{R_{TISSUE,meas}(x,y,\lambda) - R_{BG,meas}(x,y,\lambda)}{R_{SPEC,meas}(x,y,\lambda) - R_{BG,meas}(x,y,\lambda)}$$

Dark field illumination efficiently rejects specular light from the detection path and the scan lens yields normal illumination over the full FOV and illumination bandwidth. However, it also reduces the initial source intensity by nearly 50%, consequently a broadband super continuum laser (SuperK Blue, NKT Photonics, Denmark) operating at 10-12% power was used to generate sufficient signal from breast tissues with 1msec exposure times. Light from the source was coupled into a 200μm multi-mode fiber, slightly increasing the effective illumination volume reported in our initial, static beam prototype[3] (coupling the laser to smaller fibers increased speckle noise). Light scattered from a 150μm diameter spot size overlapping the illumination spot size was collimated back by the telecentric lens de-scanned and focused onto a 50μm detection fiber coupled to a CCD-based spectrometer. The focal length of the detection lens was chosen to have a lateral magnification of 0.5 so that the 50μm fiber detects light scattered within a 100μm diameter spot size on the sample plane. Signal localization limited detection to weakly scattered photons by obstructing multiply scattered light and the probability of absorption [4]. The advantage of this design is natural separation of absorption and scattering, which are quite convolved even in mesoscopic sampling volumes, although the signal only originates from the tissue surface. Measurements of tissue-simulating phantoms have demonstrated system low sensitivity to changes in hemoglobin absorption below concentrations of 60μM; hemoglobin is the dominant tissue chromophore encountered in the visible portion of the light spectrum, and is unlikely to exceed 60μM in excised breast tissues[5].

Localization of the illumination-detection sampling volumes combined with the typical values of absorption encountered in tissue, limits detection to short-pathlength photons, which are primarily influenced by scatter (pathlengths are too short to allow for appreciable absorption). This localization simplifies spectral parameterization in a complex transport regime that is neither diffuse nor single scattering, but highly sensitive to the wavelength-dependent phase function[6]. Reflectance spectra in the waveband that avoids hemoglobin peaks (610:700nm) behave with a power law dependence (on wavelength); and an empirical approximation to Mie theory was used to described the relative reflectance spectrum, $R_{TISSUE,ref}(x,y,\lambda)$, in this waveband[7]. Reflectance spectra acquired from clinically relevant breast pathologies are displayed in an inset of Figure 1. Their linear spectral shape justifies application of this simple approximation

$$R_{TISSUE,ref}(x,y,\lambda) = A(x,y)\lambda^{-b(x,y)}$$

Here, parameters A and b are defined as the scattering amplitude and scattering power, respectively. These quantities reflect variations in the size and number density of scattering centers in the volume of tissue probed, which occur on sub-micron and even sub-nanometer length scales[8-10]. The data-model fitting was log transformed and linear regression was employed to obtain estimates of the scattering amplitude and scattering power relative to Spectralon through direct matrix inversion. Additionally, a measure of average irradiance was calculated by integrating the reflectance spectrum over a waveband that avoids the hemoglobin absorption peaks (610-700 nm).

In this HIPAA-compliant, prospective study, approved by the Institutional Review Board for the protection of human subjects, written informed consent was not required for participants, although an information sheet regarding the study was provided with an opt-out provision. Fresh tissue procured during breast conserving surgery or surgical biopsy was obtained directly from the Department of Pathology at DHMC from patients who did not decline this use of their tissue. Specimen imaging did not affect procedure time in the operating room or the content and verification of the final pathology report. Tissues were imaged within one hour of resection and returned to pathology for standard histological processing. An effort was made to image larger lumpectomy specimens, typical of the tissue volumes encountered during surgery. In the case of inked lumpectomy specimens, the three-dimensional tissue volume was loafed (standard pathology protocol) and one face of one slice of tissue was imaged in a region unaffected by ink. In some cases, tissues were cut from the larger specimen. Figure (2) illustrates the protocol developed for co-registration of the imaged field with histology from the large, fresh tissue sections: a thin, paraffin window bounding the image field was placed between the tissue surface and glass plate to locate the imaged field in an inverted geometry. When the paraffin windowed tissue was removed from the optical assembly, pins dipped in India ink were placed at the corners of the imaged field to secure the specimen to a piece of cork and mark the imaged portion of the sample with black circles. The tissue-cork assembly was placed tissue-side down in 10%-formalin and fixed with the inked pins in place. After fixation, the pins were removed and the tissue was paraffin-embedded and stained with Hematoxylin and Eosin (H&E).

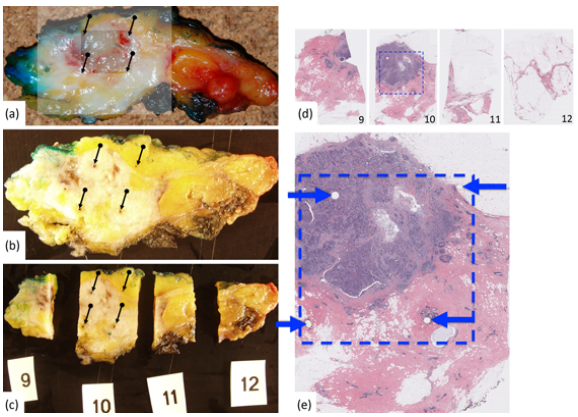

Figure 2 Co-registration between imaged field and pathology for larger, lumpectomy specimens.

Circumscribed pin marks with inked borders were clearly evident on the H&E stained sections, so that pathology correlates could be determined within areas bound by the pin markers. Figure (3) illustrates co-registration of scattering parameter maps with pathology for a benign, in situ and invasive cancer diagnosis.

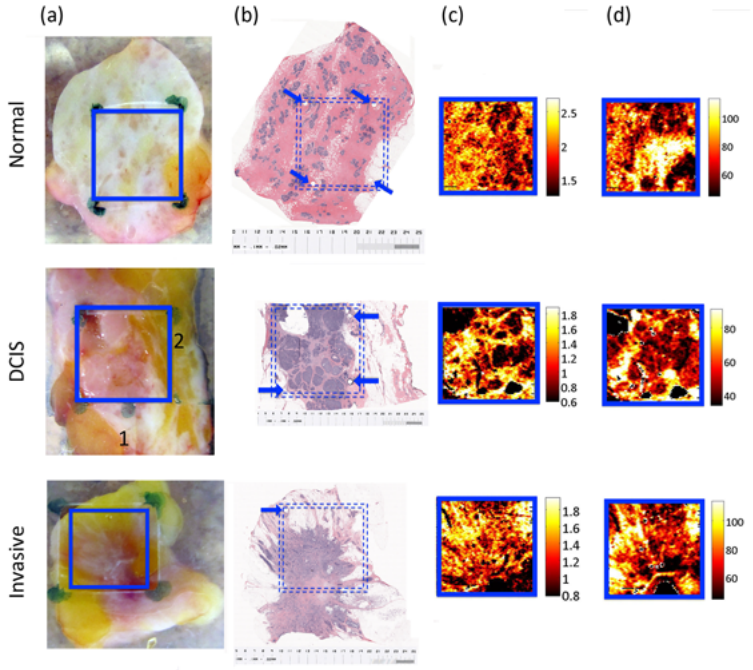

Figure 3 Spectroscopic scattering maps co-registered with pathology for key diagnostic classes.

The optical system samples mesoscopic tissue volumes; therefore, microscopic segmentation of glandular, stromal and adipose regions was not attempted within the imaged field. The 1cm^2-imaged field was assigned a microscopic diagnosis between pin markers according to pathologist interpretation (WA Wells). While breast lesions are heterogeneous at the cellular level, the illumination-detection volume was designed to strike a balance between sensitivity to cellular ultra-structure and imaging tissue fields relevant to surgical margin assessment. Image artifacts

were automatically detected; pixels with low signal-to-background or detector saturation, which occurred when insufficient contact existed between tissue and the glass plate, were removed from the image field. Specimens from a total of 32 patients were imaged with five excluded from the study – three because of insufficient contact between the tissue sample and the glass plate and two were confounded by chemotherapy treatment prior to surgery. Following automatic artifact removal, a total of 299,029 spectra were sampled from 32 FOVs in specimens acquired from 27 patients – demographics of sampled tissues and corresponding scattering parameters are detailed in Table (1). The dataset represents a significantly larger number of broadband spectra than those reported in probe-based classification studies[11].

Diagnosis	**# Patient**	**# FOV**	**# Spectra**	**Scattering Power (b)** $\mu \pm \sigma$	**Log Scattering Amplitude (A)** $\mu \pm \sigma$	**Integrated Intensity (I_{avg})** $\mu \pm \sigma$
NOR	6	8	77,033	1.72 +/- 0.21	4.89 +/- 0.45	113.52 +/- 34
FCD	5*	5	47,786	1.65 +/- 0.26	4.61 +/- 0.69	92.71 +/- 21.74
FA	6	6	54,779	1.66 +/- 0.19	4.40 +/- 0.60	51.73 +/- 13.96
DCIS	2*	2	18,601	1.04+/- 0.12	2.73 +/- 0.34	61.68 +/- 2.73
INV	9	11	100,830	1.15 +/- 0.37	3.08 +/- 1.03	70.29 +/- 17.65

Table 1 Demographics of tissues imaged and corresponding mean scattering parameters.

Box plots of spectral parameters showed distributions as a function of diagnosis and facilitated initial comparison of group medians. Discrimination was assessed between benign and malignant pathologies and between the benign pathological sub-types, normal, fibrocystic disease and fibroadenomas, and the invasive pathology sub-types, DCIS and invasive cancer. Parameter mean and standard deviation per diagnosis and per 1cm^2 FOV were calculated to quantify heterogeneity in breast tissue optical properties per patient for a given diagnosis. One-way analysis of variance was employed to assess whether parameters were drawn from a population with the same sample mean. This evaluation was followed by a paired, two-sample t-test to determine which diagnostic groups were differentiable. The Behrens-Fisher null hypothesis tested whether parameters extracted from paired diagnostic groups were drawn from independent, normal distributions with equal means, but not necessarily equal variance. Variance was not assumed to be equal between diagnostic groups based on the group box plots. For all calculations, the null hypothesis was rejected with α=0.05.

Box plots of the region-averaged scattering slope and integrated irradiance as a function of diagnosis are illustrated in Figure 4; the mean and standard deviation per diagnosis are listed in Table (1).

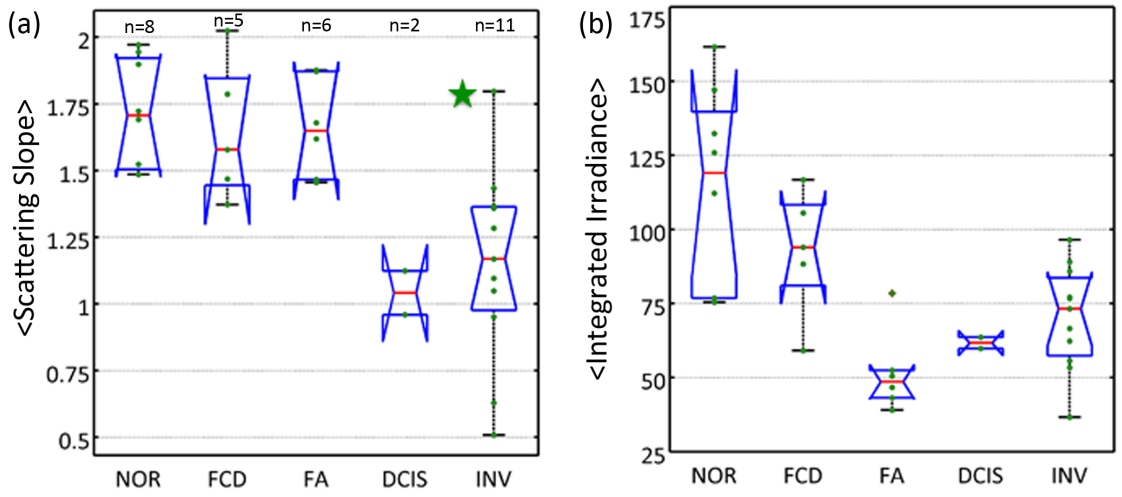

Figure 4 Box plots of fitted scattering parameters as a function of diagnosis: (a) mean scattering slope per 1cm2 FOV, (b) mean integrated irradiance per 1cm2 FOV. The green star in (a) is an indicator of the invasive cancer extreme.

The intra-patient scattering response was expectedly heterogeneous, but imaging-pathology correlates revealed that this variation had a spatial pattern that reflected the organization of glandular structures, stroma and adipose compartments. Features averaged over a $1cm^2$ FOV accounted for the inherent biological variations at this sampling resolution and a natural separation between benign and malignant pathologies emerged. Higher scattering slopes were typical of benign, as compared to in situ and invasive pathologies. This finding is consistent with literature reports of an overall decrease in the reduced scattering coefficient at all wavelengths associated with benign relative to malignant tissues[12-14]. Histology showed the invasive cancer extreme with high scattering slope (indicated by the green star in Figure 4(a) had dense stromal content, typical of normal tissues, perhaps explaining its outlier behavior. In this and previous studies, fibroadenomas were observed to have a high scattering power, but low integrated intensity[15]. Together, these parameters rendered fibroadenomas readily distinguishable.

Task 2. Develop an automated classification algorithm to provide real-time, un-biased interpretation of scatter images for improved evaluation of breast surgical margins.

Receiver operator characteristic (ROC) analysis assessed the performance of threshold-based classification of benign and malignant pathologies according to regional scattering power as a function of the number of spectra averaged per region defined by a bin size (length of each square, averaged region). This approach is advantageous as compared to the k-NN classifier reported in initial work with the prototype system because it is unsupervised, meaning it does not require population of a training feature space. Area under the curve (AUC) as a function of bin size was used to characterize the scale of morphological variance within typical breast pathologies at this resolution and to identify the region size necessary for a robust diagnosis according to scattering features. Additionally, discrimination between benign and malignant

pathologies according to average scattering irradiance was characterized to assess the value of wavelength-dependant intensity measures of scattering.

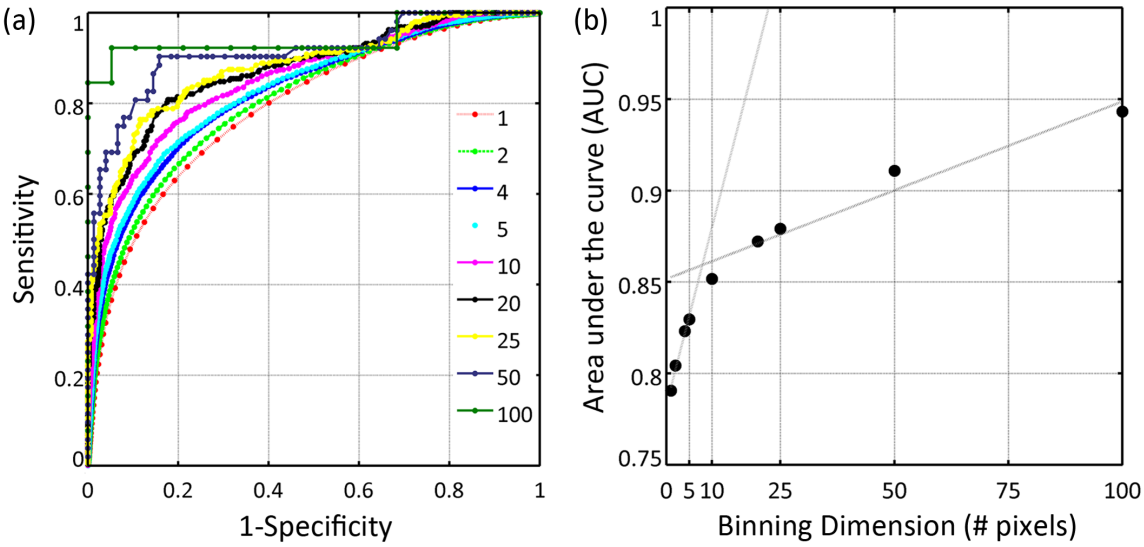

Figure 5 (a) ROC analysis of threshold-based diagnosis of benign and malignant pathologies according to region averaged scattering slope as a function of region size (bin length). (b) Area under the curve as a function of region size revealed that 10x10 spectra, or spectra sampled within a 1mm2 area, sufficiently accounted for biological variance and produced a robust diagnosis.

An understanding of signal variance relevant to morphological features within a given pathology at the detection resolution is critical to the development of spectroscopic tools for tissue diagnosis; otherwise sampling artifacts can misinform a diagnosis. The system employed here shows spatial patterns in scattering that reflect morphological features that inform pathology. ROC analysis in Figure 5 compared diagnosis of benign and malignant pathologies according to the region-averaged scattering slope as a function of region size. Region size spanned single spectra, a 100μm^2 detection spot size, to the spectroscopic image, a 1cm^2 surface area. The performance curve suggests local spectra sampled with a 1mm^2 area characterize morphological variations observed in typical breast pathologies at this resolution and renders a robust diagnosis according to scattering features. Discrimination between benign and malignant pathologies according to 1cm^2 region-averaged scattering power was achieved with 94% accuracy, 85% sensitivity, 100% specificity, 100% positive predictive value and 90% negative predictive value. When a diagnosis was rendered on a per-spectrum basis, classification was achieved with 73% accuracy, 64% sensitivity, 80% specificity, 68% positive predictive value and 77% negative predictive value; highlighting the importance of sufficiently sampling inherent biological variance at the given sampling resolution.

Task 3. Enhance the diagnostic utility of our system by investigating the micro-optical properties of breast tissue.

Textural features were explored to better understand spatial patterns in spectral light scattering from stromal and epithelial distributions. Here, a co-occurrence matrix representation was used to interpret the spatial distributions of intensities resulting from dependencies between scattering spectra (i.e., the textural features in parametric-spectral space). Examples of texture maps and corresponding pathology for benign, in situ and invasive cancer are presented in Figure 6.

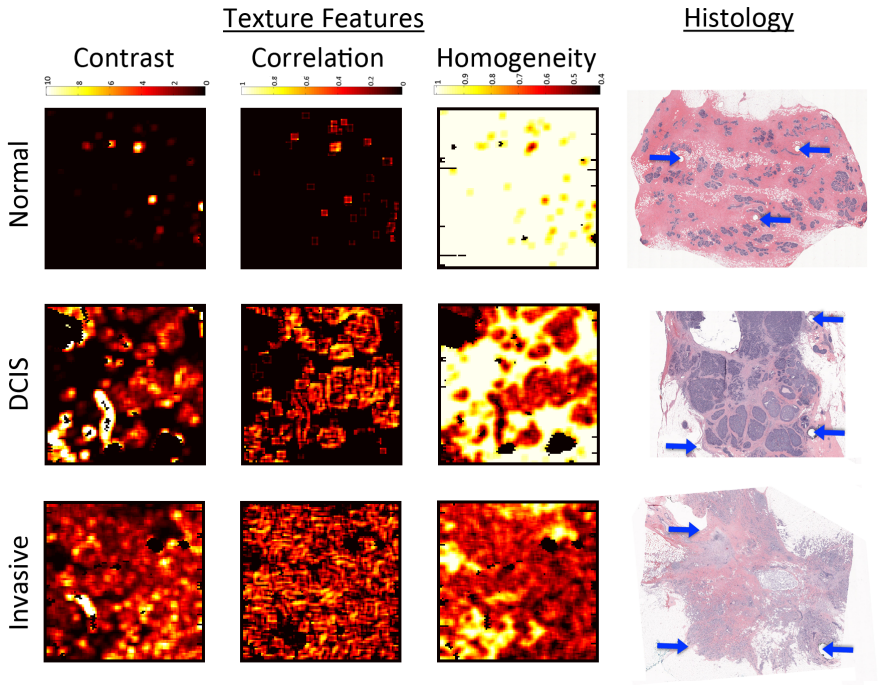

Figure 6 Textural images associated with normal (row 1), DCIS (row 3) and invasive cancer (row 5) pathologies: maps of spectroscopic textural contrast (column 1), textural correlation (column 2), and textural homogeneity (column 3) are shown. Column 4 includes the corresponding histology for the image sets with pin marks indicated by blue arrows.

The first column shows a map of the texture contrast for tissues with increasing diagnostic severity. Texture contrast is uniform and low for normal tissues, and tends to increase in its intensity and disorder for in situ carcinomas, a pathology characterized by marked expansion of glandular units by neo-plastic cells, compressing (but not invading) the surrounding stromal environment. Invasive cancers have uniformly high texture contrast, likely because of their infiltrative epithelial component. Similar trends are observed in the maps of texture correlation (column 2) and inverse trends are evident in maps of texture homogeneity. These results suggest that epithelial regions have more local variance (contrast) and exhibit some linear dependence on intensity value (correlation); mainly because the size of epithelium is near to the detection resolution. In contrast, stroma, primarily composed of collagen, is characterized by low textural variance and high homogeneity – likely because collagen fibers are two orders of magnitude smaller than the sampling resolution (~1μm in length). Box plots summarizing texture parameters as a function of diagnosis for all patients, including the shape features, Euler number

and Fractal dimension, are shown in Figure 7 and highlight the unique information provided by these measures.

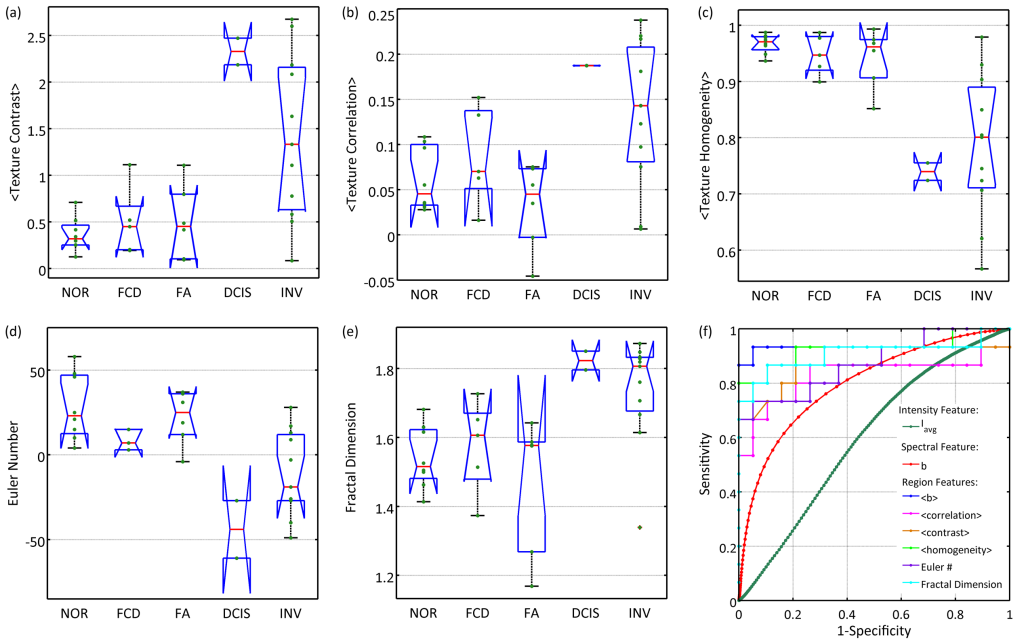

Figure 7 Box plots of textural features as a function of diagnosis: (a) scattering correlation, (b) scattering contrast, (c) scattering homogeneity, (d) Euler number, and (e) fractal dimension. (f) ROC analysis of classification of benign and malignant pathologies according to: (f1) integrated scattering irradiance, (f2) the spectral slope, b, and (f3) region-averaged, spectroscopic textural features.

To generalize, diagnostic trends observed in shape features, benign pathologies have a positive Euler number (more homogeneous) and invasive pathologies have a negative Euler number due to their local spatial variance. The high spatial variance characterizing malignant pathologies is also manifest in its fractal dimension, which approaches two (suggesting greater turbidity). Pair-wise discrimination between normal and invasive pathologies, normal and DCIS pathologies, and invasive and DCIS pathologies, are evaluated according to region-averaged spectral and textural parameters; their respective Pearson's correlation coefficients are presented in Table 2.

Paired Diagnosis	<b>	<I_{avg}>	<Correlation>	<Contrast>	<Homogeneity>	Euler #	Fractal Dimension
NOR-INV	0.0006	0.0712	0.0150	0.0046	0.0013	0.0018	0.0016
NOR-DCIS	0.0300	0.0057	6.62E-10	0.0171	0.0134	0.1468	0.0007
INV-DCIS	0.4637	0.1553	0.0452	0.0145	0.3038	0.2673	0.1437

Table 2 Pairwise discrimination between normal and invasive (NOR-INV), normal and DCIS (NOR-DCIS) and invasive from DCIS (INV-DCIS) pathologies according to spectrally derived texture features.

Significant values are underlined; note that the spatial-spectral features, correlation and contrast, are the only parameters to successfully differentiate DCIS from both benign and malignant pathologies. Differentiation of DCIS from normal tissue is more important from a clinical

standpoint, and is achieved with region-based measures within the 95% confidence limits. Even though the number of spectra collected from in situ pathologies exceeds 18,000, the data were produced from only two patients due to limited availability and prospective determination of the diagnosis. While textural features may successfully decouple in situ pathologies from their normal and invasive counterparts, specimens from a larger patient population are needed for confirmation. Textural signatures of DCIS are rather intuitive because DCIS is composed of morphological features found in both normal tissue and invasive pathologies – the spatial relationship between these scattering components is responsible for uniquely identifying the pathology in situ.

Investigation of the micro-optical properties of breast tissue using second harmonic generation (SHG) microscopy and scanning electron microscopy (SEM) was not pursued as initially planned, largely because how these properties would relate to scattering parameters specific to our imaging geometry was not clear. Further, the scattering spectrum was observed to be relatively featureless, necessarily limiting unique information obtained from its spectrum, regardless of increased transport model complexity.

Key Research Accomplishments

- A new, scanning *in situ* spectroscopy platform that selectively samples the spectrum of near-single event light scattering over a 1cm^2 FOV was developed for reduced imaged acquisition time (DAQ reduced by 85% as compared to the initial prototype system).

- Localized spectroscopic images of resected breast tissues were analyzed to characterize the spatially dependent spectral signatures of clinically relevant breast pathologies in 29 surgical breast tissues.

- Local scattering changes detected over the 1cm^2 field of view discerned benign from malignant pathologies with 94% accuracy, 85% sensitivity, 100% specificity, and positive and negative predictive values of 100% and 90%, respectively, using a simple, threshold-based classifier.

- Spectroscopic texture features were explored to encode key morphological patterns with diagnostic power; texture features suggest a unique contrast mechanism for DCIS.

Reportable Outcomes

Peer-reviewed publications

Laughney AM, Krishnaswamy V, Rizzo E, Schwab M, Barth R, Pogue BW, Paulsen KD, Wells WA, "Scatter spectroscopic imaging distinguishes breast pathologies in tissues relevant to surgical margin assessment," Clinical Cancer Research (submitted 2011).

Laughney AM, Krishnaswamy V., Garcia-Allende PB,Conde OM, Wells WA, Paulsen KD, Pogue BW, "Automated classification of breast pathology using local measures of broadband reflectance," JOURNAL OF BIOMEDICAL OPTICS (2010).

V. Krishnaswamy, **A. M. Laughney**, K. Paulsen, and B. Pogue, "A Dark-Field In Situ Scanning Spectroscopy Platform for Broadband Imaging of Resected Tissue," Optics Letters (accepted).

Conference Publications

Laughney, A., Krishnaswamy, V., Wells, W., Paulsen, K., Pogue, B., "Optical assessment of pathology in surgically resected breast cancers" Proceedings of SPIE BiOS Conference, Biomedical Applications of Light Scattering V, San Francisco CA, January 2011.

Laughney, A., Krishnaswamy , V., Garcia-Allende, P.B., Wells , W.A., Conde, O.M., Paulsen, K.D., Pogue, B.W., "Imaging Breast Pathology in situ using Broadband Scatter Spectroscopy and a K-Nearest Neighbor Classifier," Proceedings of the OSA BIOMED Conference, Bio-optics in clinical application, Miami FL, April 2010.

Presentations

"A spatially-modulated scatter imaging system to detect tumor-associated stroma," *Breast Tumor Board Conference at Dartmouth-Hitchcock Medical Center, Spring 2011.*

"Optical characterization of pathologies in surgically resected breast cancers," Biomedical Lecture Series, Thayer, Spring 2011.

"System design for optical characterization of tissue pathologies in situ," *NSF ADVANCE Workshop at Rice University, Fall 2010.*

"Optimizing spectral contrast in breast lesions relative to normal tissue for surgical guidance," *Thayer, Spring 2010.*

"Automated Classification of Breast Pathology using Local Measures of Broadband Reflectance," *Optical Society of America 2010 BIOMED Conference (Miami, Fl), Spring 2010; Beckman Institute at the University of California Irvine, Winter 2009.*

Research Opportunities Received

2011 Biophotonics International Graduate Summer School
NSF ADVANCE Workshop at Rice University
Pathobiology of Cancer Workshop by the American Association of Cancer Research
Neukom Institute Travel Grant

Conclusions

In this study, spectroscopic images of resected breast tissues were analyzed to characterize the spatially dependent spectral signatures of clinically relevant breast pathologies. Images were acquired using a scanning *in situ* spectroscopy platform that rapidly samples the spectrum of near-single event light scattering over a $1cm^2$ FOV, significantly decoupling the effects of absorption from scattering and allowing linear interpretation of the resulting spectra. Spatially, the intra-specimen scattering response was expectedly heterogeneous, but imaging accounted for this morphological diversity and improved region-based diagnosis. Analysis of performance curves as a function of region size revealed that spectroscopic measures within a $1mm^2$ area sufficiently characterized the morphological variance typical of breast pathologies at this sampling resolution and rendered a robust diagnosis according to scattering features. Local scattering changes detected over the $1cm^2$ field of view discerned benign from malignant pathologies with 94% accuracy, 85% sensitivity, 100% specificity, and positive and negative predictive values of 100% and 90%, respectively, using a simple, threshold-based classifier. The texture features of correlation, contrast and homogeneity, and the shape features of fractal dimension and Euler number, significantly discriminated benign from malignant pathologies, indicating that scattering variation encodes key morphological patterns with diagnostic power. In a limited patient data set, texture features identified ductal carcinoma in situ within 95% confidence limits, suggesting potential contrast mechanisms for this clinically important, yet challenging pathology to detect intra-operatively. The system was designed to strike a balance between sensitivity to cellular morphology and imaging fields that account for inherent diversity within a diagnosis for eventual use as a diagnostic adjunct during surgery.

References

1. Krishnaswamy V, Laughney AM, Paulsen KD, Pogue BW: **Dark-field scanning in situ spectroscopy platform for broadband imaging of resected tissue**. *OPTICS LETTERS* 2011, **36**(10):1911-1913.
2. Ti Y, Lin W-C: **Effects of probe contact pressure on in vivo optical spectroscopy**. *OPTICS EXPRESS* 2008, **16**(6):4250-4262.
3. Krishnaswamy V, Hoopes PJ, Samkoe KS, O'Hara JA, Hasan T, Pogue BW: **Quantitative imaging of scattering changes associated with epithelial proliferation, necrosis, and fibrosis in tumors using microsampling reflectance spectroscopy**. *JOURNAL OF BIOMEDICAL OPTICS* 2009, **14**(1):014004.
4. Pogue BW, Burke G: **Fiber-optic bundle design for quantitative fluorescence measurement from tissue**. *APPLIED OPTICS* 1998, **37**(31):7429-7436.
5. Krishnaswamy V, Laughney AM, Paulsen KD, Pogue BW: **A Scanning In Situ Spectroscopy Platform for Imaging Morphological Contrast in Lumpectomy Specimens**. *OPTICS EXPRESS* 2011 (under review).
6. Kanick SC, Gamm UA, Schouten M, Sterenborg HJCM, Robinson DJ, Amelink A: **Measurement of the reduced scattering coefficient of turbid media using single fiber reflectance spectroscopy: fiber diameter and phase function dependence**. *Biomedical optics express* 2011, **2**(6):1687-1702.
7. Vanstaveren HJ, Moes CJM, Vanmarle J, Prahl SA, Vangemert MJC: **Light-Scattering in Intralipid-10-Percent in the Wavelength Range of 400-1100 Nm**. *APPLIED OPTICS* 1991, **30**(31):4507-4514.
8. Backman V, Gopal V, Kalashnikov M, Badizadegan K, Gurjar R, Wax A, Georgakoudi I, Mueller M, Boone CW, Dasari RR *et al*: **Measuring cellular structure at submicrometer scale with light scattering spectroscopy**. *IEEE JOURNAL OF SELECTED TOPICS IN QUANTUM ELECTRONICS* 2001, **7**(6):887-893.
9. Perelman LT, Backman V, Wallace M, Zonios G, Manoharan R, Nusrat A, Shields S, Seiler M, Lima C, Hamano T *et al*: **Observation of periodic fine structure in reflectance from biological tissue: A new technique for measuring nuclear size distribution**. *PHYSICAL REVIEW LETTERS* 1998, **80**(3):627-630.
10. Subramanian H, Pradhan P, Liu Y, Capoglu IR, Li X, Rogers JD, Heifetz A, Kunte D, Roy HK, Taflove A *et al*: **Optical methodology for detecting histologically unapparent nanoscale consequences of genetic alterations in biological cells**. *P Natl Acad Sci USA* 2008, **105**(51):20118-20123.
11. Nachabe R, Evers DJ, Hendriks BHW, Lucassen GW, van der Voort M, Rutgers EJ, Peeters M-JV, Van der Hage JA, Oldenburg HS, Wesseling J *et al*: **Diagnosis of breast cancer using diffuse optical spectroscopy from 500 to 1600 nm: comparison of classification methods**. *JOURNAL OF BIOMEDICAL OPTICS* 2011, **16**(8):087010.
12. Ghosh N, Mohanty S, Majumder S, Gupta P: **Measurement of optical transport properties of normal and malignant human breast tissue**. *Appl Opt* 2001, **40**:176 - 184.
13. Palmer G, Zhu C, Breslin T, Xu F, Gilchrist K, Ramanujam N: **Monte Carlo-based inverse model for calculating tissue optical properties. Part II: Application to breast cancer diagnosis**. *Appl Opt* 2006, **45**:1072 - 1078.
14. Kennedy S, Geradts J, Bydlon T, Brown JQ, Gallagher J, Junker M, Barry W, Ramanujam N, Wilke L: **Optical breast cancer margin assessment: an observational study of the effects of tissue heterogeneity on optical contrast**. *BREAST CANCER RESEARCH* 2010, **12**(6):R91.
15. Laughney AM, Krishnaswamy V, Garcia-Allende PB, Conde OM, Wells WA, Paulsen KD, Pogue BW: **Automated classification of breast pathology using local measures of broadband reflectance**. *J Biomed Opt* 2010, **15**(6):066019.